ESC-TR-92-143

(2)

Project Report
SWP-6
Revision 1



# SWAT Laboratory Test Results

R.R. Parenti
D.V. Murphy

10 March 1993
(Originally Issued 16 January 1989)

**Lincoln Laboratory**
MASSACHUSETTS INSTITUTE OF TECHNOLOGY
*LEXINGTON, MASSACHUSETTS*

Prepared for the Department of the Air Force under Contract F19628-90-C-0002.

This report is based on studies performed at Lincoln Laboratory, a center for research operated by Massachusetts Institute of Technology. The work was sponsored by the Air Force Phillips Laboratory under Air Force Contract F19628-90-C-0002.



The ESC Public Affairs Office has reviewed this report, and it is releasable to the National Technical Information Service, where it will be available to the general public, including foreign nationals.

This technical report has been reviewed and is approved for publication.

FOR THE COMMANDER

Gary Tutungian
Administrative Contracting Officer
Directorate of Contracted Support Management

MASSACHUSETTS INSTITUTE OF TECHNOLOGY
LINCOLN LABORATORY

# SWAT LABORATORY TEST RESULTS

*R.R. PARENTI*
*D.V. MURPHY*
*Group 54*



**PROJECT REPORT SWP-6**
**Revision 1**

**10 MARCH 1993**





LEXINGTON MASSACHUSETTS

# ABSTRACT

The non-cooperative-target beam-control problem has been the subject of intense investigation since the synthetic-beacon concept was first introduced to the high-energy-laser community in 1982. While numerous analytical studies and computer simulations have been performed to evaluate the practical utility of this phase-measurement technique, prior to Lincoln Laboratory's SWAT (Short-Wavelength Adaptive Techniques) program no experimental verification had been obtained. In the first phase of the SWAT investigation, completed in 1985, a high degree of correlation between differential-phase measurements from natural and artificial sources was demonstrated.

The next phase of the SWAT program will be performed at the AMOS (Air Force Maui Optical Station) facility in Maui, where a 241-actuator adaptive-optics system and an array of six dye lasers will be integrated with the site's 60-cm beam director. Prior to shipment, the adaptive-optics subsystem was subjected to a thorough laboratory evaluation, which culminated in a series of compensation tests involving simulated beacon sources. The results of these measurements are in good agreement with theoretical predictions and provide strong evidence of the efficacy of the synthetic-beacon approach.

# PREFACE

From 1982 to 1991 Lincoln Laboratory was supported by the Defense Department to develop the technology of uncooperative-target adaptive optics. A principal feature of this program was the development of synthetic beacons as the reference source for the adaptive-optics wavefront sensor. This technique overcame problems associated with point-ahead and target brightness.

In the late 1980's it became clear that synthetic-beacon technology could be of great value to the astronomical community, who routinely deal with dim objects. Moreover the basic concept had been reinvented by the astronomers with, apparently, no input from the US Defense community. The civilian community seemed on the verge of embarking on a major development program duplicating work the US Government had already paid for.

It seemed incumbent therefore on the DoD to provide to the astronomers the wealth of information that had been developed over the past decade. So, in May 1991 the US Air Force released virtually all of the development work and associated documentation. The immediate impact was that Defense workers began to present their material in open publication. We are now moving to republish a number of documents that seem of greatest import. To some extent these documents are dated as far as military work is concerned, but they are likely to be of great value to the astronomers. At a minimum they are of historical and archival significance.

The report that follows is one of many documents we are in the process of releasing. The original report numbered SWP-6 ("SWAT Laboratory Test Results," dated 16 January 1989) is now updated. If you possess the original, it should be destroyed in accordance with current document-control procedures. We are providing a copy of this report to the Defense Technical Information Center (DTIC) so that users may request it. There are intended to be no distribution limitations on this document.

# TABLE OF CONTENTS

# LIST OF ILLUSTRATIONS

# LIST OF TABLES

# 1. INTRODUCTION

The non-cooperative-target beam-control problem has been the subject of intense investigation since the concept of using synthetic beacons as atmospheric probes was introduced to the high-energy-laser community in 1982. The proposed solutions typically involve the placement of one or more focused beams in the target's point-ahead direction (the so-called "A" method approach) or the projection of a single collimated beam that is laterally sheared ("S" method). While numerous analytical studies and computer simulations have been performed to evaluate the practical utility of uncooperative-compensation techniques, direct experimental verification will require a major hardware-development effort and an ambitious measurements program.

To this end, Lincoln Laboratory has undertaken a series of field experiments that are collectively referred to as the SWAT (Short-Wavelength Adaptive Techniques) program. The first phase, in which the differential subaperture tilt produced by a synthetic beacon and that produced by a star were compared in a pair of subapertures, was successfully completed in FY85. The next set of experiments will be performed at the AMOS (Air Force Maui Optical Station) facility in Maui, and will integrate a 241-actuator adaptive-optics system and an array of six dye lasers with the site's 60-cm beam director.[1] This instrumentation has been specifically designed to evaluate single and multiple-beacon A-method deployment schemes, but provision has also been made to perform a limited set of sheared-beam tests.

As of this writing, all of the adaptive-optics components and one of the six dye lasers for the SWAT II experiments have been installed at the Maui site. Prior to shipment, the adaptive-optics subsystem was subjected to a thorough laboratory evaluation, which culminated in a series of atmospheric-compensation tests involving simulated beacon sources. The stated objectives included a demonstration of multiple-beacon phase correction in a simulated turbulence environment.

---

[1] R. R. Parenti, P. N. Everett, R. Kramer, and D. A. Page, "SWAT II Overview," Lincoln Laboratory Project Report SWP-3 (Revision 1) (November 1992).

This report summarizes the results of the SWAT laboratory experiments and compares the measured performance with that predicted by current theory. To the best of our knowledge, these data represent the most nearly definitive experimental verification of the synthetic-beacon concept obtained to date.

# 2. DESCRIPTION OF LABORATORY EQUIPMENT

This section presents a brief overview of the SWAT laboratory hardware. A major concern in designing this equipment was the accuracy with which the gross atmospheric effects that give rise to focal anisoplanatism could be represented. A good simulation of a typical atmosphere was achieved by constructing an optical path having two sets of phase screens appropriately positioned with respect to the receiving aperture. Also incorporated were light sources at scaled ranges of 10 km and infinity, as well as a means to shutter those sources to duplicate the action of a range-gated beacon laser. All dynamic sequencing functions and data recording operations were performed under the direct control of a microVAX computer system.

## 2.1 OPTICAL LAYOUT

In the baseline SWAT field tests, a set of pulsed-dye lasers will be used to project a total of five synthetic beacons, one placed at the center of the receiving aperture and four others centered over each of four aperture sections. For passive scoring tests, a sixth source, usually a bright star, will provide a means to characterize the quality of the phase correction.

All of the essential aspects of beacon geometry, phase sensing, wavefront compensation, and far-field scoring were incorporated into the design of the SWAT laboratory. A simplified diagram of the optical layout is given in Figure 2-1. The six sources representing the beacons and the scoring star were produced by a pair of CW argon-ion lasers operating at 514.5 nm. The light from one of the lasers was collimated; the other beam was split into five components that were laterally displaced to form the desired spot pattern and that could be individually controlled with mechanical shutters. In order to limit the path length required to simulate the effects of 10-km sources, the receiving aperture was demagnified to a diameter of 1.5 cm, thus producing a scaling factor (designated by $\beta$) of 40 with respect to the 60-cm aperture at AMOS. Scaling laws for the critical simulation parameters are summarized in the table below.

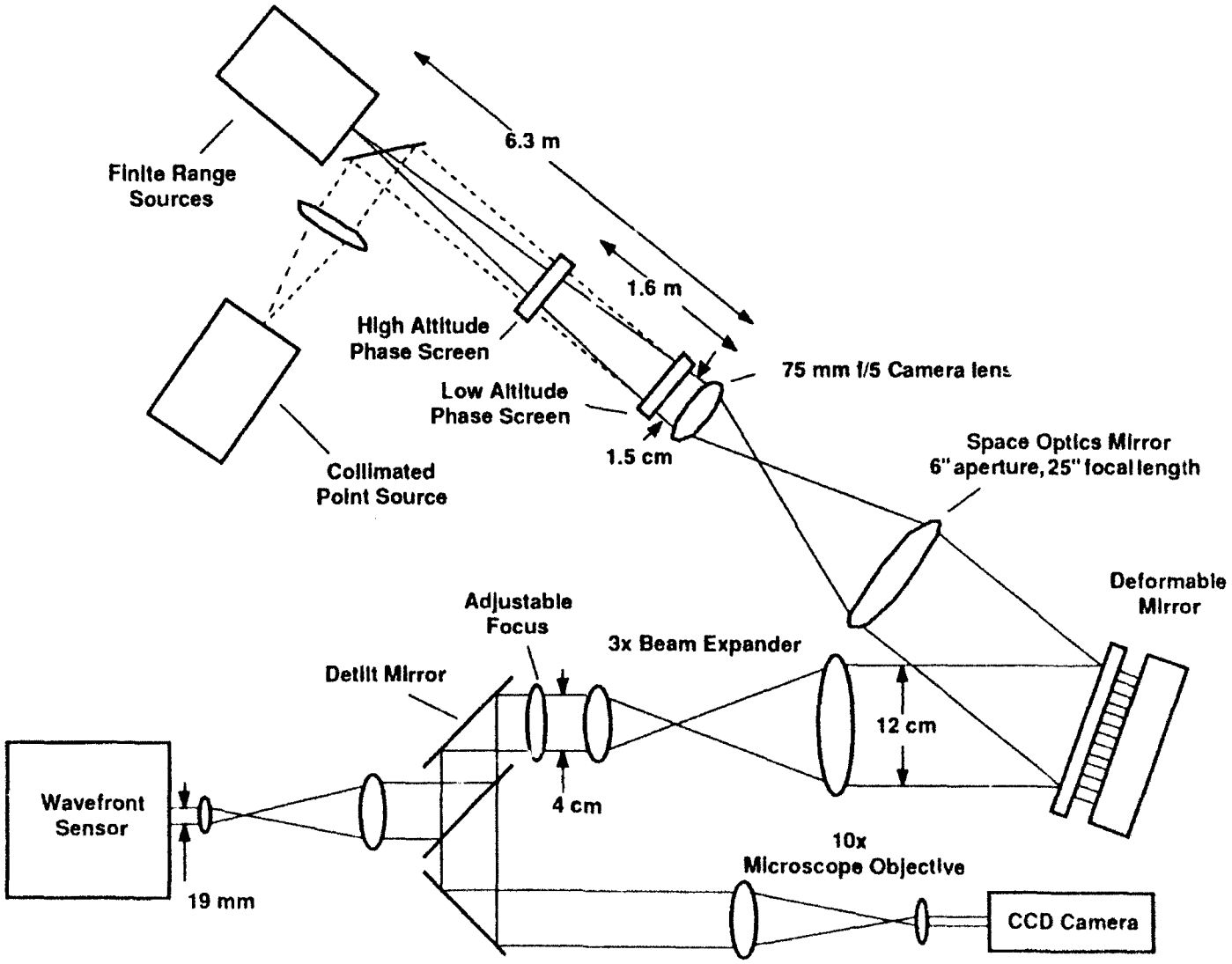


*Figure 2-1. Laboratory layout.*

**TABLE 2-1**
**Scaling Factor Summary**

| | |
|---|---|
| Collection Aperture Diameter | $1/\beta$ |
| Range Parameters | $1/\beta^2$ |
| Phase Screen Strengths | $\beta^{5/3}$ |

Using this geometry, the path length from the sources to the receiver could be reduced to just over 6 meters.

Wavefront control in the laboratory was accomplished just as it will be in the field - by a 241-actuator deformable mirror driven by a modified-Hartmann phase sensor. A digital reconstructor was used to convert the phase-gradient outputs from the wavefront sensor to a set of optimal actuator positions for phase conjugation. All actions were closely synchronized with the timing of the wavefront sensor and far-field camera, as described in the next section.

## 2.2 EXPERIMENT CONTROL AND DATA RECORDING

The most significant differences between the laboratory and field hardware configurations are apparent in the design of the control and recording subsystems. In order to minimize complexity and provide replacements for components still under construction, all timing functions for the laboratory tests were handled by a hard-wired sequencer directed by a microVAX computer. As shown in Figure 2-2, the sequencer sends control pulses to the beam shutters, tilt mirror, wavefront sensor, deformable mirror, and CCD camera in the proper order. The timing diagram for this process is shown in Figure 2-3. The phase-correction cycle

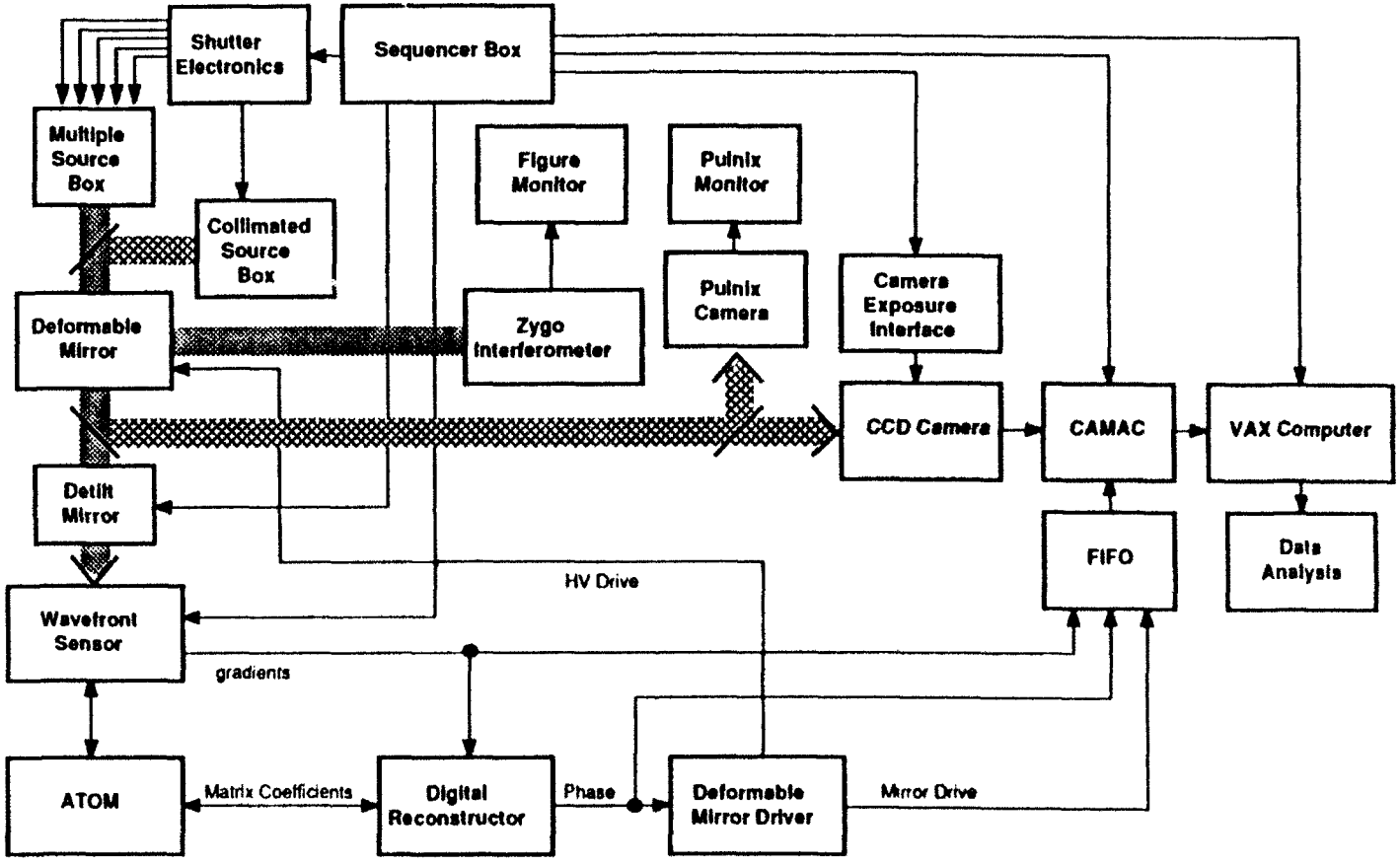


*Figure 2-2. Laboratory experiment control system.*

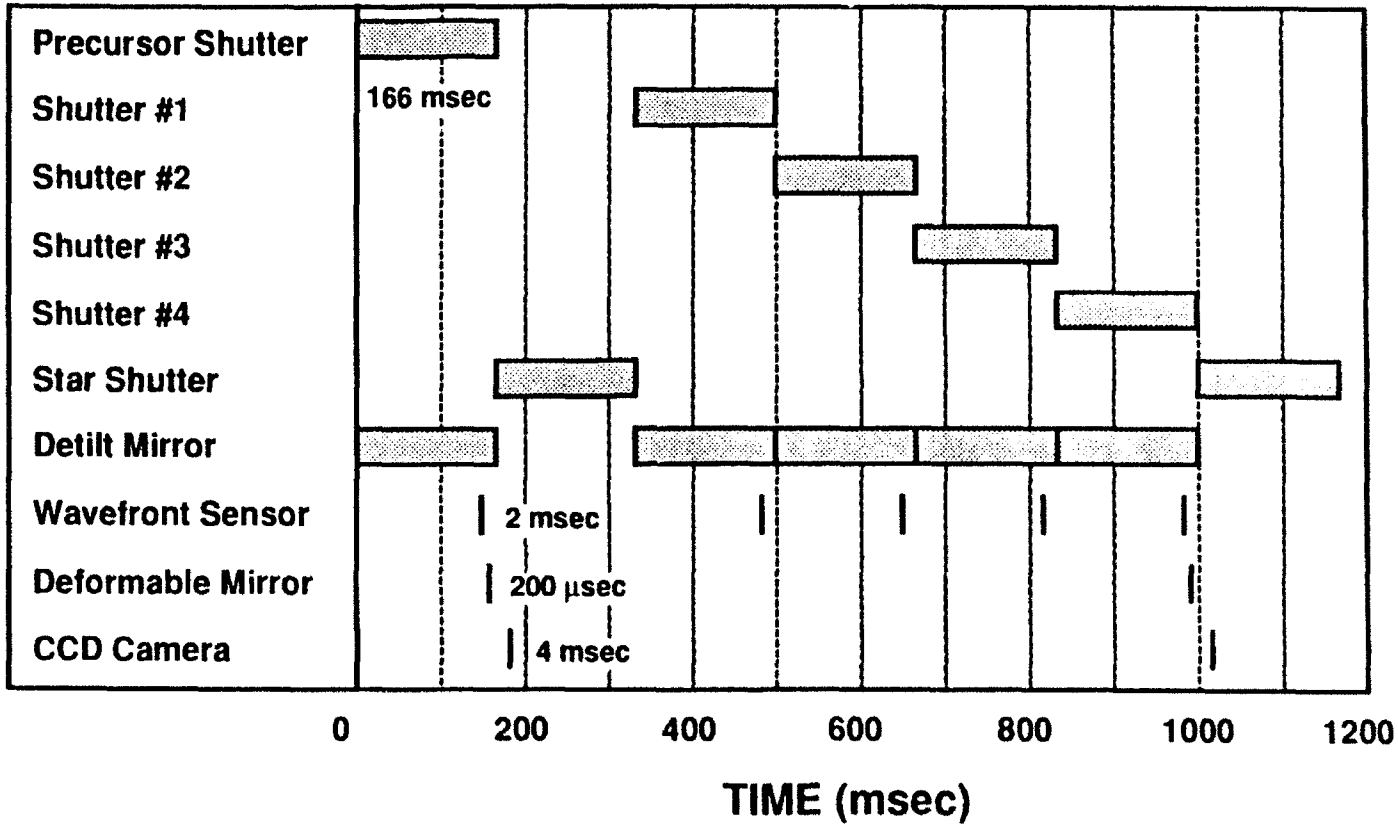


*Figure 2-3. Multiple-source laboratory experiment baseline sequence.*

is completed in approximately 1.2 seconds. This cycle can be repeated indefinitely for CW loop-closure experiments. Since the sequencer is equipped with discrete parallel outputs, the order in which the various beams are shuttered is easily modified by rearranging the output connections.

The microVAX system shown in Figure 2-2 serves both as a trigger for the sequencer unit and as a data-storage medium. Upon command from the system operator, a data *session* consisting of a series of sequential *experiments* is initiated, with all essential data recorded onto a hard disk. Usually 40 experiments, each following the timing sequence shown in Figure 2-3, were performed. The associated records include the following information:

- x and y phase gradients for each beacon sample
- x and y intensities for each beacon sample
- reconstructed phases
- phase drive voltages
- two sets of CCD camera images

All of this information is archived according to date and time and is also immediately available for analysis through the local VAX network. Derived parameters, such as those listed below, can be readily generated and presented in either text or graphics format:

- minimum, maximum, and average gradient values
- gradient curls
- minimum, maximum, and average intensities
- minimum, maximum, and average phase values
- minimum, maximum, and average CCD camera pixel values
- far-field Strehl ratios

## 2.3 PHASE SCREEN CHARACTERIZATION

To correlate the observed performance with that predicted by our computer simulations, a good characterization of the phase screens used in the laboratory tests is essential. During most of the tests, one or more screens from a set of three were placed in the beam path at the positions indicated in Figure 2-1. Digitized phase maps for each of these screens were obtained using a high-resolution (100 x 100) Zygo interferometer. Structure functions derived from these images, scaled to a 60-cm aperture, are presented in Figure 2-4. The anticipated shape of the tilt-removed structure function for Kolmogorov turbulence is given by the expression

$$D_{\varphi z}(r) = 51.3\ \sigma_f^2\ (r/D)^{5/3}\ [1-(r/D)^{1/3}] \quad . \tag{2-1}$$

A plot of this function for a figure variance $\sigma_f^2 = 3.7\ \text{rad}^2$ is included in Figure 2-4. All three of the measured curves are seen to be close to the correct form, with the match for Screen #1 being particularly good. Coherence diameter, isoplanatic angle, and log amplitude fluctuation values for these screens are derived from the figure variance as follows:

$$\text{Coherence Diameter} = \qquad r_o = 0.299\ D/(\sigma_f^2)^{3/5} \quad , \tag{2-2}$$

$$\text{Isoplanatic Angle} = \qquad \vartheta_o = 0.0942\ D/h_o(\sigma_f^2)^{3/5} \quad , \text{and} \tag{2-3}$$

$$\text{Log Amplitude Fluctuation} = \qquad \sigma_\chi^2 = 9.90\ (h_o/kD^2)^{5/6}\ \sigma_f^2 \quad . \tag{2-4}$$

where $h_o$ represents the altitude of the phase screen. On this basis, the following tabulation is given. (In the bench simulation the screens were placed in one of two positions - a so-called low-altitude position that was adjacent to the entrance aperture, or a high-altitude position for which $h_o \approx 2.8$ km. The $\vartheta_o$ and $\sigma_\chi^2$ numbers apply to the placement of screens at the high-altitude position.)

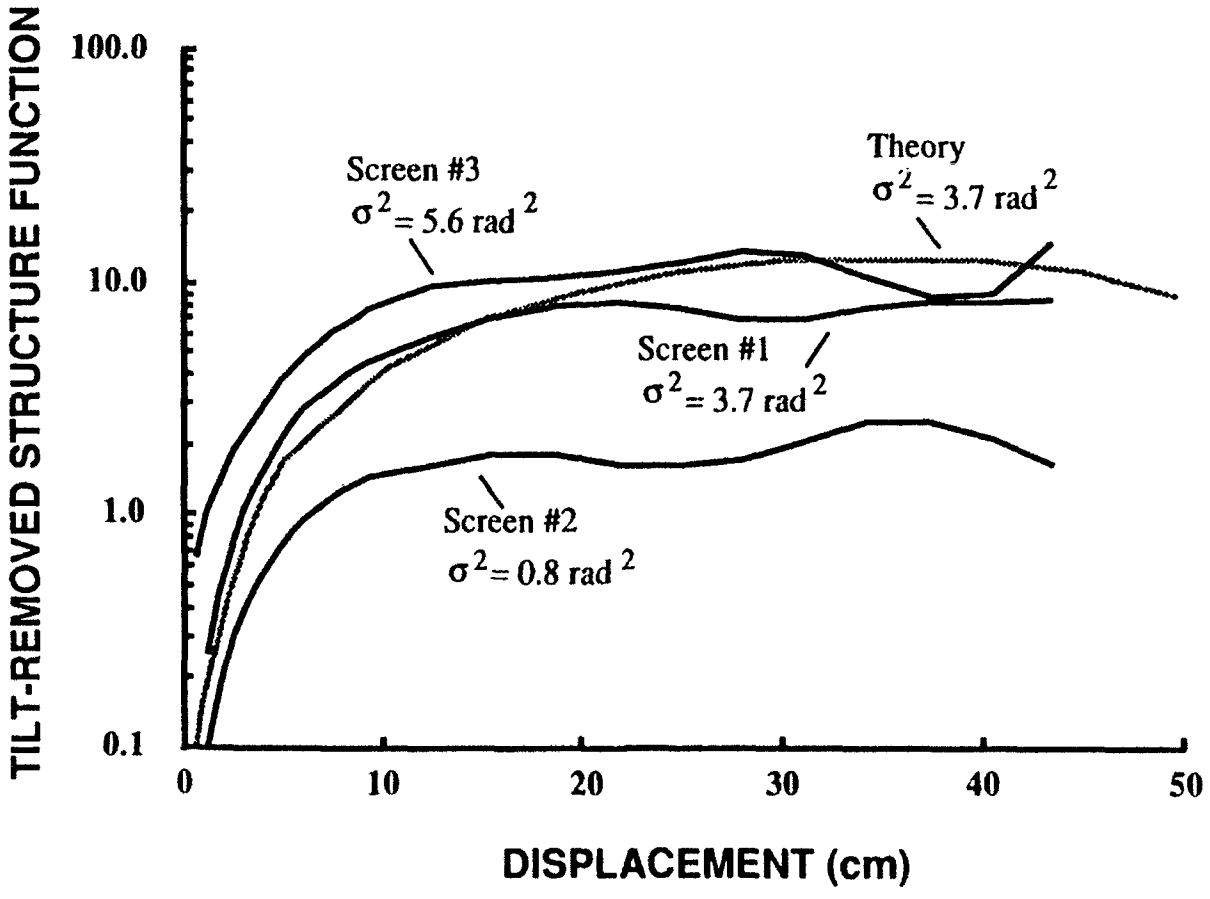


*Figure 2-4. Phase screen structure function analysis.*

**TABLE 2-2**

**Phase Screen Parameter Summary**

| | $\sigma_f^2$(rad$^2$) | $r_o$(cm) | $\vartheta_o$ (μrad) | $\sigma_\chi^2$ (Nepers$^2$) |
|---|---|---|---|---|
| Screen #1 | 3.7 | 8.2 | 9.2 | 0.08 |
| Screen #2 | 0.8 | 20.5 | 23.0 | 0.02 |
| Screen #3 | 5.6 | 6.4 | 7.2 | 0.12 |
| Screens #1 & 2 | 4.5 | 7.3 | 8.2 | 0.10 |
| Screens #1, 2, & 3 | 10.1 | 4.5 | 5.0 | 0.22 |

It can be seen that a wide range of turbulence conditions could be readily simulated by adjusting the number and position of the included screens.

# 3. RECENT THEORETICAL RESULTS

Central to the SWAT experiments is the question of achievable Strehl as a function of such parameters as beacon size, number, and altitude. Several numerical studies relevant to the SWAT configuration have been conducted in the last few years, with beacon-size effects having been recently added. These investigations typically incorporate atmospheric models consisting of ten or more phase screens and apply geometrical ray-tracing to develop a phase-error function for each atmospheric realization. Statistical mean and uncertainty values are obtained by running multiple realizations for each engagement scenario. For small deviations from a nominal geometry, the error variance for focal anisoplanatic effects will scale as

$$\sigma^2_{\text{focal anisoplanatism}} \propto (D/H\vartheta_0)^{5/3} \quad , \tag{3-1}$$

where D and H represent the aperture diameter and beacon altitude respectively. Reasonably accurate Strehl estimates can be obtained from the error variance results through the use of the extended Marèchal approximation.

A summary of some recent numerical results for the SLC-Day atmospheric model and the SWAT 60-cm aperture is given in Figure 3-1. The lowest curve shows the expected Strehl as a function of beacon altitude for a single beacon geometry and illustrates the deleterious effects of focal anisoplanatism. As the source altitude is reduced, errors are incurred as a result of the unsampled turbulence above the beacon and the incorrectly sampled atmosphere below the beacon. The use of multiple beacons improves the low-altitude sampling and can, as indicated by the middle curve, produce a significant Strehl improvement. One of the principal tasks of the SWAT field experiments is to measure the performance difference between the single-beacon and four-beacon sampling geometries.

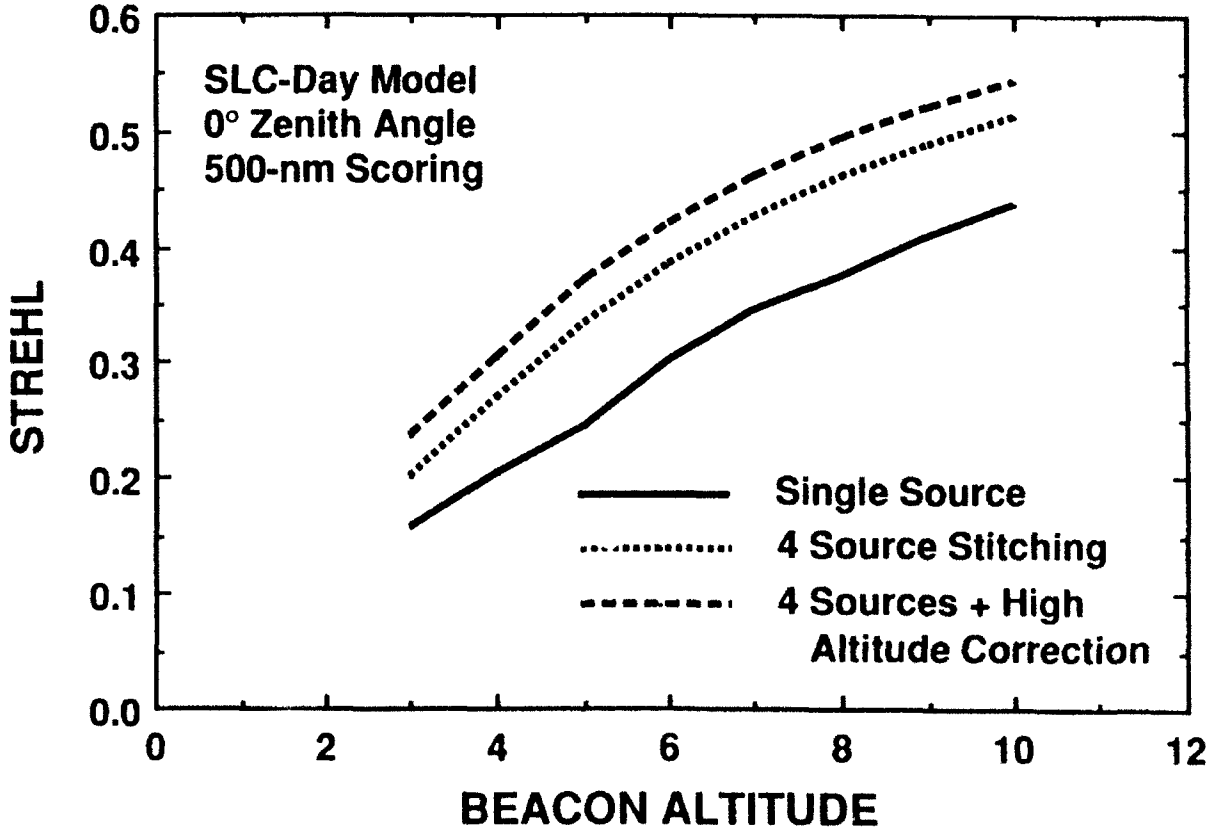


*Figure 3-1. SWAT performance curves for the SLC-Day model.*

Numerical simulations of the multiple-beacon reconstruction process have consistently demonstrated that the theoretical performance limit cannot be achieved with a single-altitude beacon configuration. Errors due to the improper measurement of high-altitude, low-spatial frequency turbulence components become increasingly more important as the size of the beacon array is enlarged. The upper-most curve in Figure 3-1 describes the performance of a source geometry known as hybrid sampling, in which residual section-tilts are corrected using a low-spatial frequency measurement of the resonant return from the earth's sodium layer at 90 km. For the SWAT system, hybrid sampling is expected to yield a small but measurable performance advantage.

As described in Section 2, the laboratory tests were specifically designed to permit Strehl comparisons to be made for a variety of source arrangements. Although the performance data generated in this manner may be compared with the theoretical results just described, a more direct measure of the fidelity of the experiment is obtained by analyzing the specific atmospheric realization achieved on the optical bench. To this end, each of the phase screens used in the experiment was mapped with the aid of a Zygo interferometer, and the resulting phase arrays were applied to the numerical stitching model.

Figure 3-2 shows a phase measurement of one of the phase screens (Screen #1) and its associated anisoplanatic error when placed at the high-altitude turbulence position on the laboratory bench. Far-field beam profiles computed through a Fourier transform of wavefront functions for a diffraction-limited beam, a point-source 10-km beacon, and an extended-beacon geometry are given in Figures 3-3a, b, and c respectively. The Strehls derived from the last two images are 0.36 and 0.42. It will be shown in the next section that these numbers are in excellent agreement with the Strehl measurements obtained from the laboratory far-field camera data.

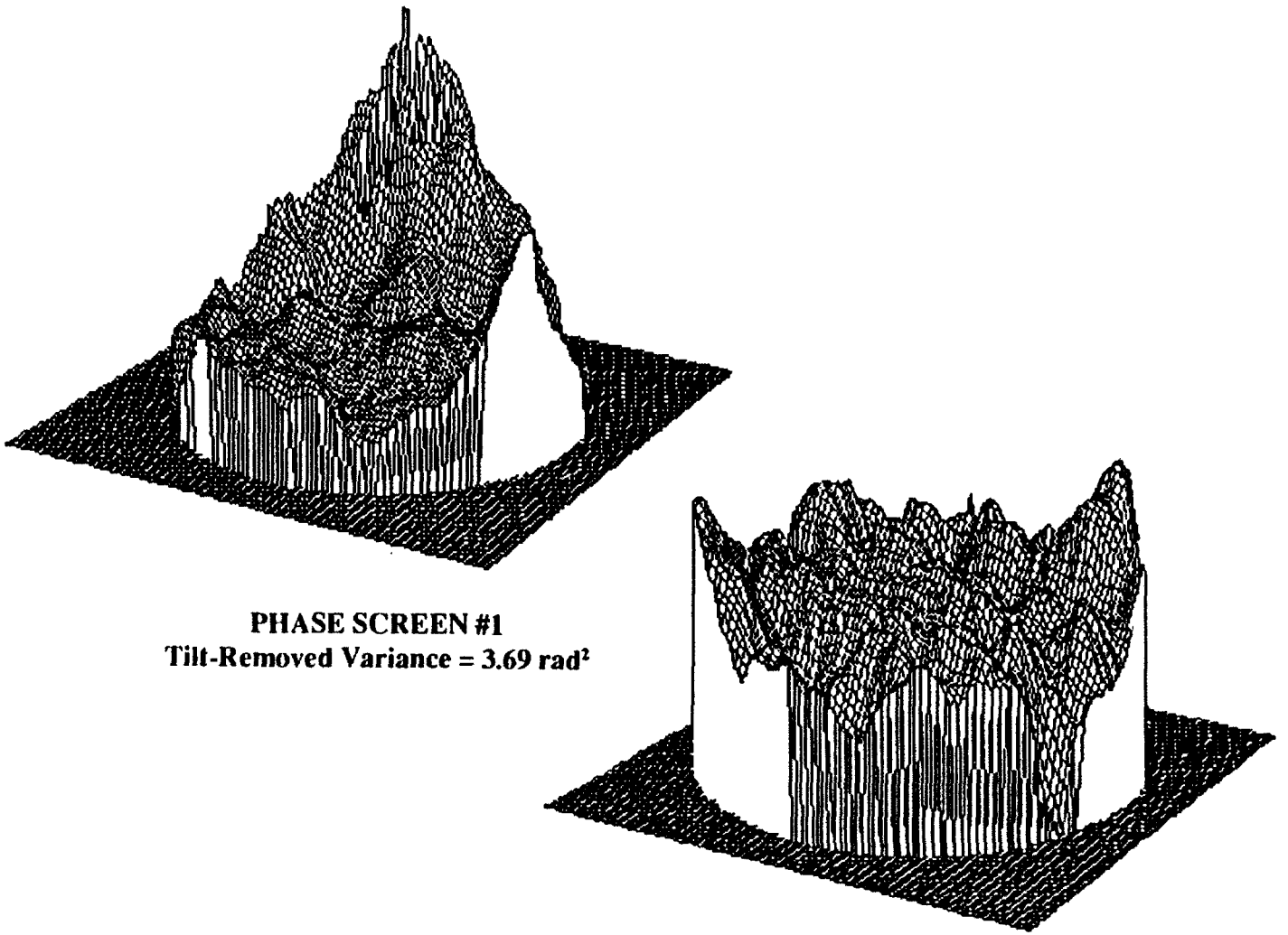


*Figure 3-2. Measured phase contours derived from Screen #1.*

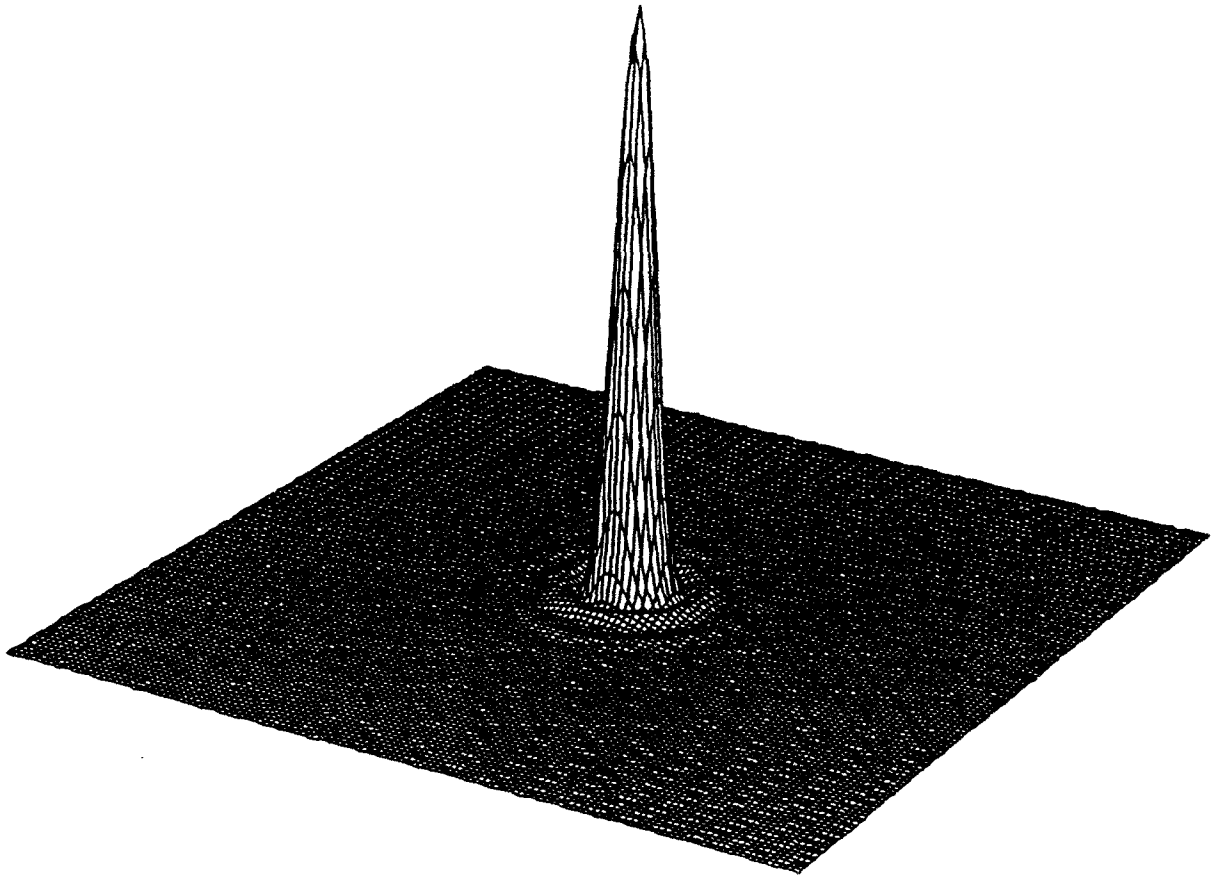

*Figure 3.3a. Diffraction-limited far-field beam profile.*

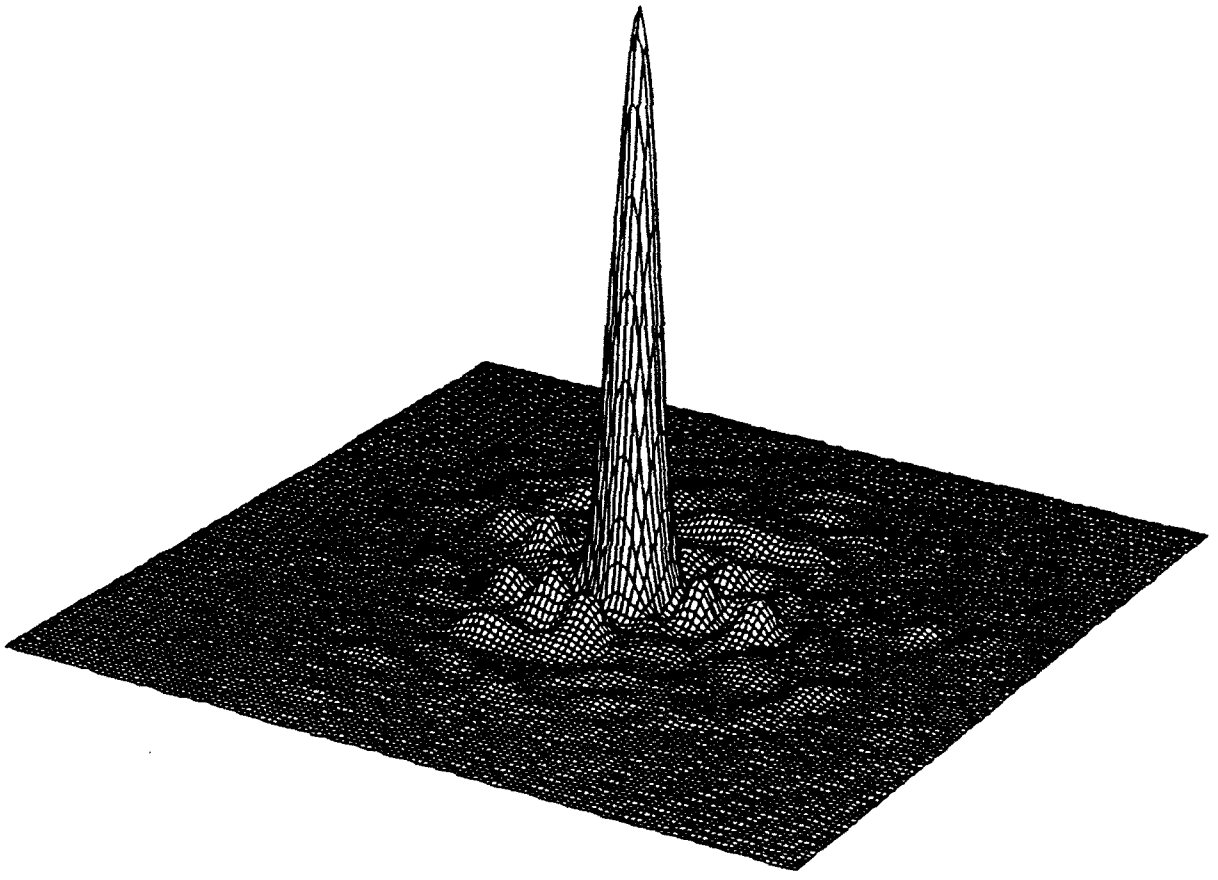

*Figure 3.3b. Far-field beam profile for a single source at 10 km and propagation through Screen #1 (Strehl = 0.36).*

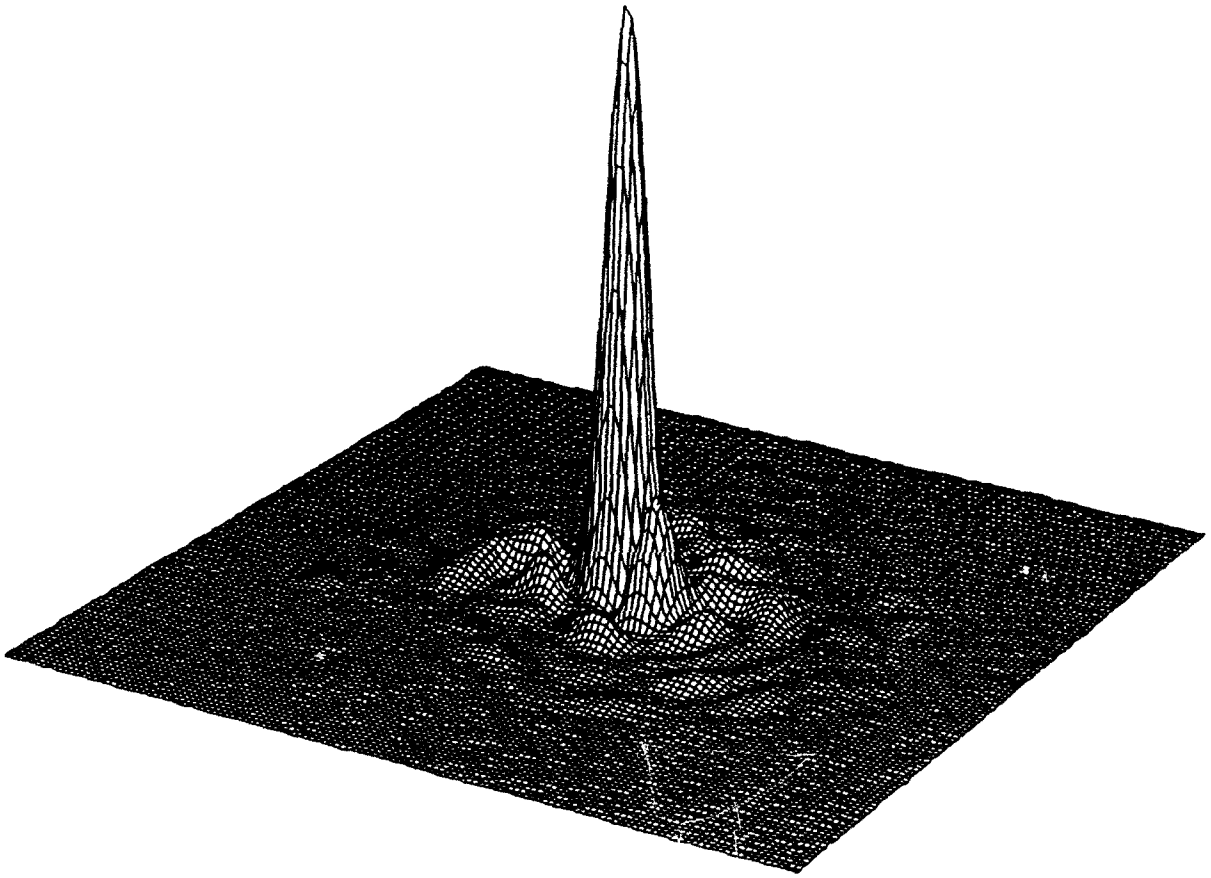

*Figure 3.3c. Far-field beam profile using a four-source-average reconstructor with 10-km beacons and propagation through Screen #1 (Strehl = 0.42).*

# 4. CW PHASE COMPENSATION RESULTS

High quality phase-compensation data had been generated on a semi-routine basis in the SWAT laboratory since the early fall of 1987, but the most reliable multiple-beacon results were obtained in the first month of 1988. During that period, a concerted effort was made to follow a procedure that would allow direct comparisons to be made with the computer predictions described earlier. To this end, a laboratory methodology incorporating the following measures was instituted.

- The beam path was carefully shielded to reduce dynamic turbulence that would be uncorrectable at the 0.5-2 Hz update rates used in these tests. In previous measurements it was found that this precaution was effective in reducing dynamic turbulence to a tolerable level.
- Far-field background frames were recorded frequently.
- Phase screen transmission measurements were made to allow for accurate throughput normalization.
- The effective system focal length into the far-field camera was computed by measuring the spot motion as a function of input wavefront tilt.
- Frequent closed-loop measurements were made without phase screens in the beam path to establish a static-aberration calibration.
- All phase screens were masked to ensure the use of the same sections throughout the tests, and the screens were independently characterized with a Zygo interferometer.

Most of the tests performed involved the placement of Screen #1 at either the low-altitude or high-altitude turbulence position. The matrix of experimental parameters is summarized in the table below.

**TABLE 4-1**
**Experimental Parameters**

| *Screen #1 Position* | *CCD Camera Source* | *Phase Sensor Source* | *Reconstruction Algorithm* |
|---|---|---|---|
| Not Placed | Collimated | Collimated | Single Source (conventional) |
| Low Altitude | | 1 at 10 km | 4 Sources, Tilt Included |
| High Altitude | | 4 at 10 km | 4 Sources, Tilt Removed |
| | | | 4-Source Average |

The last column, containing the reconstructor algorithm listing, is actually incomplete, in that it does not explicitly include all of the variations tested during this period. It was determined early in these tests that reconstructors that ignored section-tilt errors performed poorly, as did those with small section-overlap regions; performance with these obviously inferior reconstructors will not be reported.

Before proceeding with the final data presentation, it is of interest to describe some of the factors that would tend to limit the achievable Strehl. Some of the more obvious sources of non-correctable error are listed below.

- poor optical alignment
- uncorrectable common-path static aberrations
- non-common-path phase aberrations
- insufficient signal into the wavefront sensor
- inadequate mirror update rate

Considerable care was taken in the optical alignments, which were performed daily, and the use of optical intensifiers insured a high signal level into the wavefront sensor. The mirror update rate was admittedly low (0.5-2 Hz), but the optical path was well shielded from external disturbances. Of perhaps greater concern is the strong static astigmatic error, indicated in Figure 4-1, that was found in the common-path optics, and the uncertain quality of the non-common path optics into the CCD camera. The cumulative effect of these errors is difficult to quantify at this time.

Detailed analysis was performed on a set of 12 data sessions, each containing at least 30 mirror update experiments. Strehl ratios were computed in accordance with the techniques described in the Appendix to this report. For the optical arrangement in which the phase sensor viewed the collimated source, the far-field magnification constant was determined to be 3.35 pixels of displacement per wave of tilt over the full aperture. This factor, applied to Equation (A-9), yields the following Strehl expression

$$S = 14.3 \frac{Z(\text{peak}) - Z_b(\text{peak})}{\sum\sum [Z(x, y) - Z_b(x, y)]} \quad : \text{collimated source} \quad , \tag{4-1}$$

where Z and $Z_b$ represent the signal and background far-field image data. The magnification constant was slightly modified when the main focus element was adjusted to allow the phase sensor to view the 10-km sources. Since this action changed the focus in the common path, a compensating adjustment at the CCD camera was also necessary. Although a direct measurement of tilt sensitivity was not made subsequent to these adjustments, an estimate based on a comparison of well-compensated beam profiles indicates that the effective focal length into the CCD camera was increased by about 19% , so that

$$S = 20.1 \frac{Z(\text{peak}) - Z_b(\text{peak})}{\sum\sum [Z(x, y) - Z_b(x, y)]} \quad : 10 \text{ km source} \quad . \tag{4-2}$$

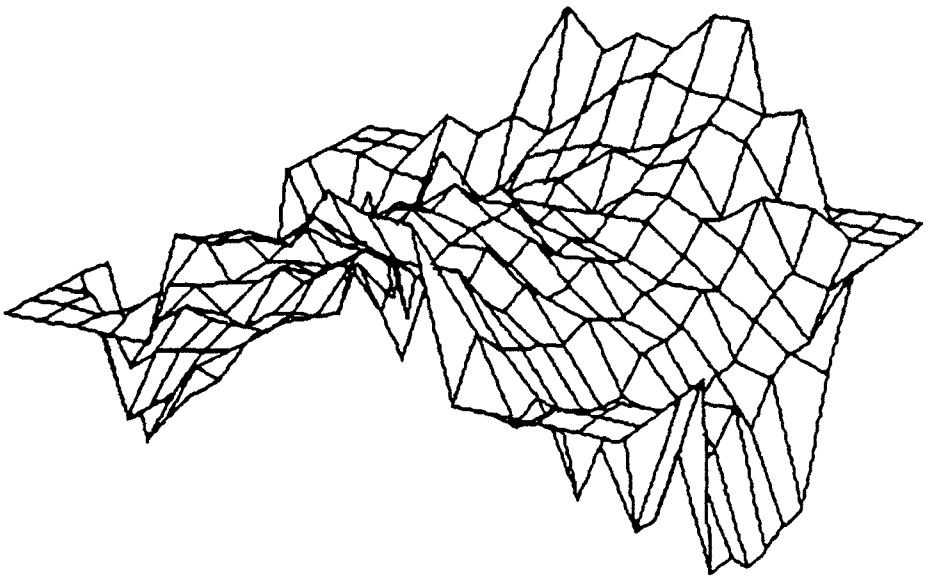

*Figure 4.1 Static aberration for the closed-loop experiments (2.7 waves peak-to-peak).*

The performance limit for the system can be determined from the far-field data collected with the non-aberrated optical path and the collimated-beam reference. The measured Strehls for this arrangement are plotted as a function of mirror update iteration in Figure 4-2. (The time interval between experiments was approximately 0.75 sec and a loop gain of 0.25 was employed.) The steady-state Strehl is seen to reach a value of just under 0.8 near the end of the sequence, which corresponds to an wavefront error of about $\lambda/13$. During this same period, the tilt-removed static mirror figure was found to be constant to better than $\lambda/40$. These observations are consistent with either a large non-common path error or the system's inability to compensate for the static aberration shown in Figure 4-1.

A performance summary for the closed-loop laboratory experiments is presented in Table 4-2. For each of the listed configurations, a Strehl prediction taken from Table 2-2 is given in the seventh column, and a measured Strehl representing an ensemble average over at least 15 experiments is shown in the last column.

The first three rows of Table 4-2 relate to configurations in which the phase sensor viewed the collimated beam while the position of phase Screen #1 was varied. Focal anisoplanatic effects will not be observed in these cases, and only losses due to fitting error and scintillation should be important. An excess phase error of the order of $\lambda/13$ is observed for all of the collimated beacon experiments.

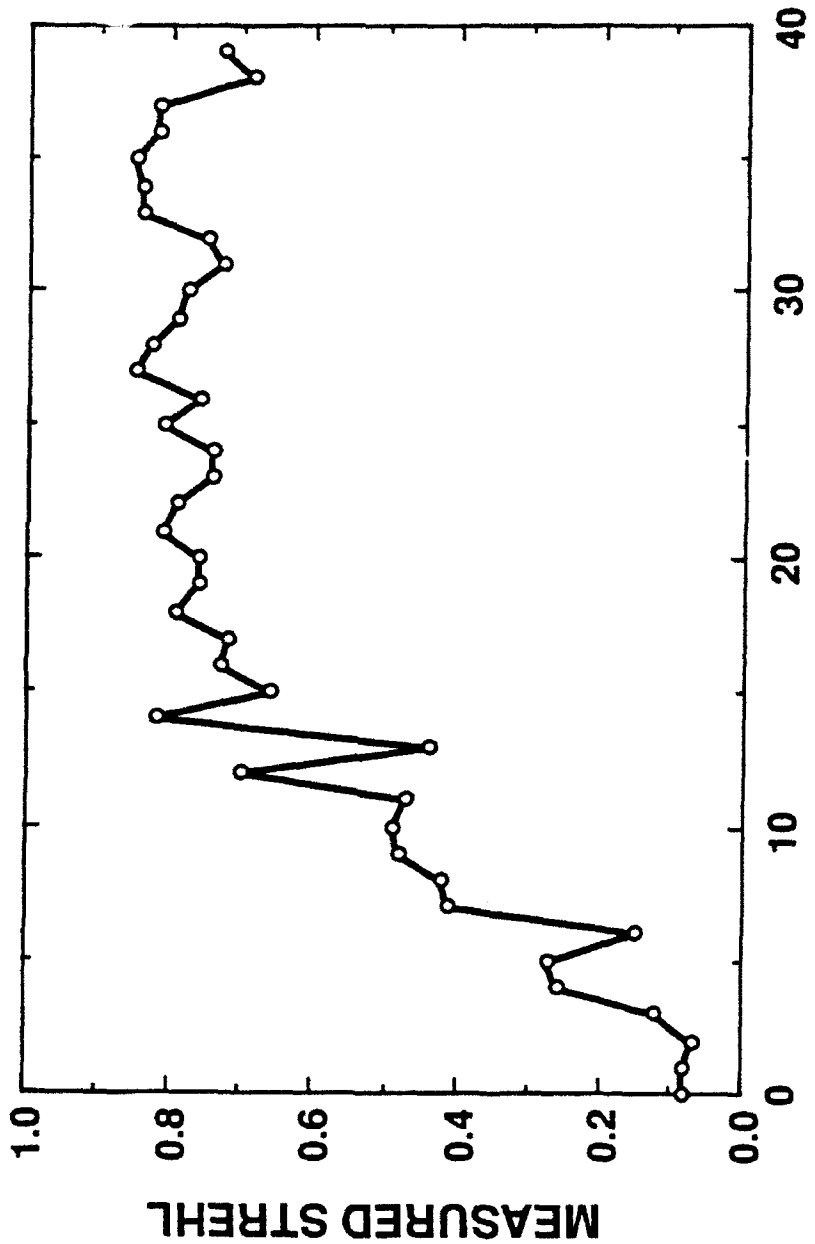


*Figure 4-2. Strehl plot for Session SWAT01161654.*

**TABLE 4-2**

**Summary of Closed-Loop Results**

| File | Configuration | Screen | Errors | $\Delta\sigma^2$ | Cum. $\sigma^2$ | Strehl | |
|---|---|---|---|---|---|---|---|
| | | | | | | Theory | Measurement[†] |
| 1654 | Star Source<br>Single-Source Reconstructor | None | None | 0.00 | 0.00 | **1.00** | **0.78** |
| 1904 | | Low | Fitting | 0.08 | 0.08 | 0.92 | 0.78 |
| 1801 | | High | $\sigma_\chi^2$ | 0.08 | 0.16 | 0.85 | 0.62 |
| 1709 | Single Source (10 km)<br>Single-Source Reconstructor | None | None | 0.00 | 0.00 | 1.00 | 0.75 |
| 1917 | | Low | Fitting | 0.08 | 0.08 | 0.92 | 0.72 |
| 1813 | | High | $\sigma_\chi^2$<br>Focal | 0.08<br>1.50 | 1.66 | **0.36**[††] | **0.36** |
| 1725 | 4 sources (10 km)<br>Average of Gradients | None | None | 0.00 | 0.00 | 1.00 | 0.82 |
| 1928 | | Low | Fitting | 0.08 | 0.08 | 0.92 | 0.76 |
| 1830 | | High | $\sigma_\chi^2$<br>Focal | 0.08<br>1.25 | 1.41 | **0.42**[††] | **0.40** |
| 1720 | 4 sources (10 km)<br>Tilt-Removed Stitching | None | None | 0.00 | 0.00 | 1.00 | 0.82 |
| 1924 | | Low | Fitting | 0.08 | 0.08 | 0.92 | 0.74 |
| 1824 | | High | $\sigma_\chi^2$<br>Focal | 0.08<br>1.15 | 1.31 | | **0.40** |

[†] Measurement error is estimated to be ±5%

[††] Simulation result using measured phase error for Screen #1

The last nine rows of Table 4-2 provide an overview of the system's operation when simulated Rayleigh beacons were positioned at a scaled altitude of 10 km. Six of these configurations were either free of intentional aberrations or employed a single phase screen near the pupil plane. Focal anisoplanatic effects should be negligible under these conditions, and, indeed, the measured Strehls are found to be essentially identical to those obtained when the wavefront sensor viewed the collimated reference laser.

The more interesting comparisons of performance achieved in the presence of focal-anisoplanatic distortion induced by high-altitude turbulence are addressed in the summaries for data files SWAT01161813, 1830, and 1824. As discussed in the last section, Strehl predictions for the first two of these configurations were obtained from numerical ray-trace simulations incorporating the same beacon geometries, screen placements, and reconstruction algorithms used in the experiment. In addition, the phase distortion used in the program was derived from a Zygo measurement of Screen #1. The agreement between the computer results and the laboratory measurements appears to be excellent. It should be noted, however, that the variations in Strehl over the sampled ensemble were large (see Figure 4-3), corresponding to an uncertainty of approximately ±0.05.

Although the data listed in this table were generated from just a single turbulence realization, both the strength and spectral characteristics of this phase screen are thought to be representative of a typical atmosphere. All of the low-altitude beacon results are judged to be consistent with earlier predictions based on the SLC-day turbulence model, and the difference between the single-beacon and four-beacon Strehls, although modest, was not unexpected. In view of these results, it is likely that much of the work to be conducted at Maui will be devoted to Rayleigh scattering from altitudes below 5 km, where the effects of focal anisoplanatism are more significant.

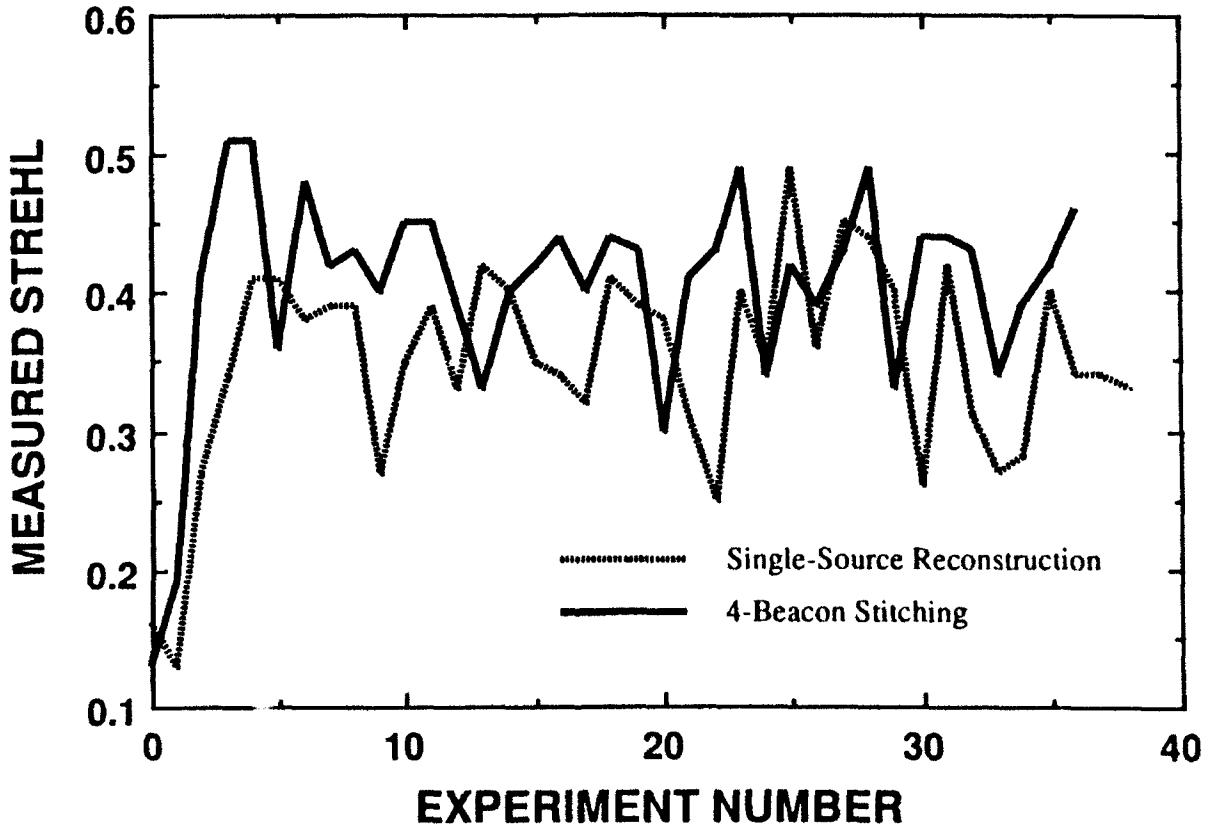


*Figure 4-3. Strehl plots for Sessions SWAT01161813 and SWAT01161824 (loop gain = 0.5).*

# 5. PULSED COMPENSATION PERFORMANCE

The beacon lasers to be used in the SWAT II tests will operate at a repetition rate that is much lower than the atmospheric time constant, thus making it impossible to perform closed-loop phase correction. The returns from each pulse must be accurately sensed, manipulated, and transformed into phases that can be applied to the deformable mirror. In this mode, calibration errors become much more important and may even become the dominant source of error. For this reason, the SWAT equipment was designed to be easily and frequently calibrated and provision was made to accommodate non-linear conversion functions.

In order to test the functionality of the system in its pulsed or "go-to" mode, the deformable-mirror loop gain was set to unity, and far-field camera measurements were made immediately after a single mirror-update cycle. The timing sequence was similar to that to be used in the field, allowing only a millisecond for the completion of the phase sampling, reconstruction, and mirror correction. A performance summary comparing the pulsed and closed-loop modes is shown the table below and in Figure 5-1. All of the data were generated using a single collimated reference beacon.

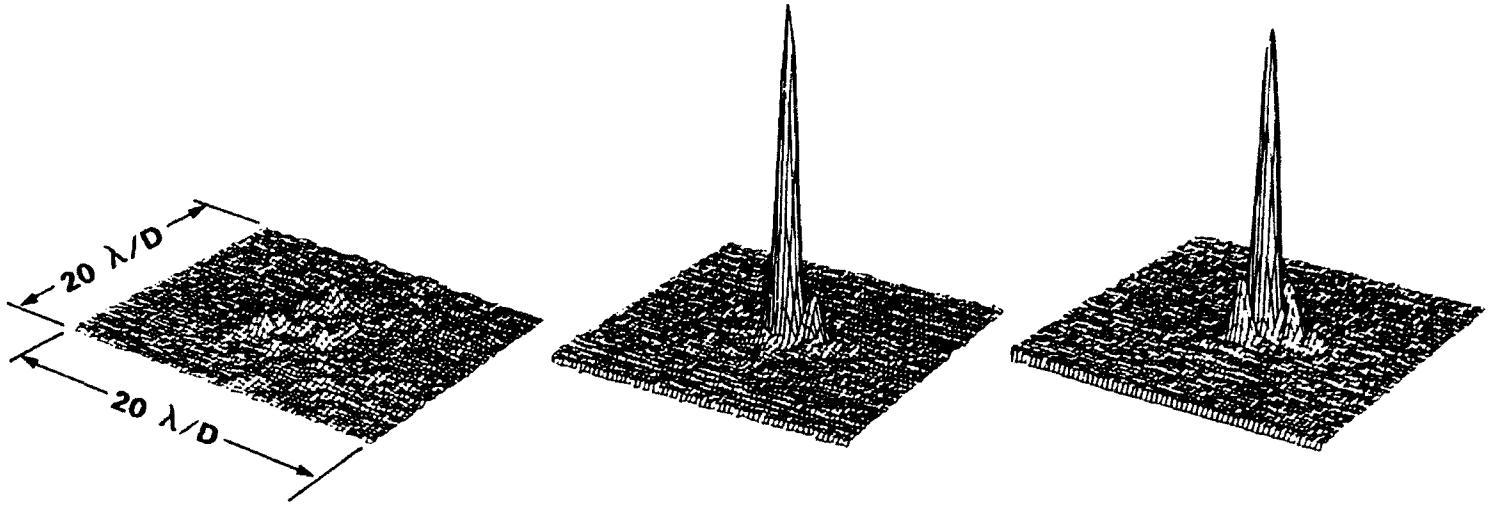


*Figure 5-1. Single pulse compensation.*

## TABLE 5-1

**Pulsed Operation Summary**
**(Files 1949, 1952, 2003, & 2005)**

| *Turbulence Conditions* | *Closed-Loop Operation* | | *Pulsed Operation* | |
|---|---|---|---|---|
| | rms Phase Fluctuation (waves) | Strehl | rms Phase Error (waves) | Strehl |
| Static Aberration | 0.04 | 0.65 | 0.08 | 0.63 |
| Phase Screen #1 | 0.05 | 0.65 | 0.08 | 0.60 |

A comparison of the closed-loop and pulsed-mode results shows the performance estimates to be nearly identical. Since these test were conducted under relatively strong turbulence conditions, they represent a fairly convincing end-to-end demonstration of pulsed-mode functionality. This experiment will undoubtedly be repeated during the field integration and testing process.

# 6. SUMMARY

The Lincoln Laboratory SWAT program represents a unusually ambitious attempt to gauge the effectiveness of a diverse set of synthetic-beacon concepts. The laboratory tests conducted in January 1988 were intended to exercise the key elements of the adaptive-optics subsystem, the data-collection equipment, and the data-analysis software. It was also hoped that these experiments would provide an initial performance evaluation of single and multiple-beacon phase-compensation techniques that could be quantitatively compared with current theory.

In all of these aspects the experiments are judged to have been successful. In particular, the agreement between theory and experiment in the closed-loop operational mode was excellent in essentially every beacon configuration. Successful correction was obtained in the single-pulse, "go-to" mode, with resulting Strehl ratios only slightly worse than obtained with CW, closed-loop compensation.

# APPENDIX:
# FAR-FIELD IMAGE ANALYSIS

The processing methods used to extract estimates of Strehl from far-field imagery are typically reviewed at the beginning of each new field exercise, and the SWAT experiments have been no exception. Over the years a wide variety of approaches have been developed to deal with this problem, all of which display a fairly high susceptablity to data normalization errors. Following a careful preliminary analysis of the data obtained during the SWAT laboratory exercise, a new approach has been devised that appears to be somewhat better suited to this task. The process comprises two distinct stages: during the first step the raw data are carefully corrected to remove fixed-pattern noise and stray light effects; in the second step an estimate of the peak irradiance value is obtained from an energy distribution function. The essential elements of this process are outlined below.

The high-resolution CCD cameras used in the SWAT program can provide two-dimensional beam images of extremely high quality. The raw output data Z(x,y) can be modeled as follows

$$Z(x,y) = \tau_d \, \tau_o \, d^2 \, g(x,y) \, E(x,y) + Z_b(x,y) \quad , \tag{A-1}$$

where E and Z represent the input optical irradiance and the electrical output signals respectively, $\tau_d$ is the camera dwell time, $\tau_o$ is the optical throughput, d is the pixel dimension, g is the the camera gain, and $Z_b$ is the fixed-pattern background. The background is normally assumed to be spatially varying but temporally static so that the $Z_b$ term can be eliminated by subtracting camera frames taken with the input light blocked. It is further assumed that the gain is independent of pixel location but that it, and the system throughput, cannot be accurately measured. Therefore, the optical irradiance function at the camera focal plane bears the following relationship to the output data

$$E(x,y) = (1/\gamma) \, [Z(x,y) - Z_b(x,y)] \tag{A-2}$$

where $\gamma$ is indeterminate. Therefore, a direct radiometric determination of the Strehl ratio is precluded but a reasonably accurate estimate can be obtained if the diffraction-limited beam

profile for the collection aperture can be computed. In general, a parameter having the form

$$\frac{Z(x,y) - Z_b(x,y)}{\sum_x \sum_y [Z(x,y) - Z_b(x,y)]}$$

will be generated at some point in the process, which eliminates the $\gamma$ term. This energy normalization is less straightforward than it appears, owing to the difficulty of simultaneously achieving high spatial resolution across the beam while obtaining an accurate measure of the total flux. Separate narrow and wide field-of-view detectors can be used for this purpose, but care must be taken to establish an accurate mutual calibration of the two sensors.

## A.1 BASELINE CORRECTION

Failure to properly subtract the fixed-pattern background noise is the greatest potential source of error in the Strehl calculation, since a baseline offset on the order of 0.1% of the peak pixel intensity can translate into a 10% error in the estimate of the total beam energy. An offset error will occur when the ambient lighting changes between the data and background frames or when the camera is exposed to signal light scattered from optical elements within its field of view.

Recall that the $Z - Z_b$ operation is intended to produce a data field that is free from fixed-pattern errors. Assuming that the focused beam subtends only a small fraction of the total detector array area, a histogram of $Z - Z_b$ should display a Gaussian peak centered at zero. Any displacement of this peak from the null position, as illustrated in Figure A-1, is evidence of a baseline offset that should be corrected.

Baseline compensation entails the formation of the quantity $I(x,y) \equiv Z(x,y) - Z_b(x,y) - Z_o$, where $Z_o$ is the computed mean of the baseline peak of the $Z - Z_b$ irradiance histogram. While the absolute value of $Z_o$ is typically small, the Strehl measurement error is proportional to the product of $Z_o$, and the number of pixels in the detector array. The implementation of this simple procedure has significantly improved the frame-to-frame uniformity of the Strehl computations performed on the SWAT laboratory data.

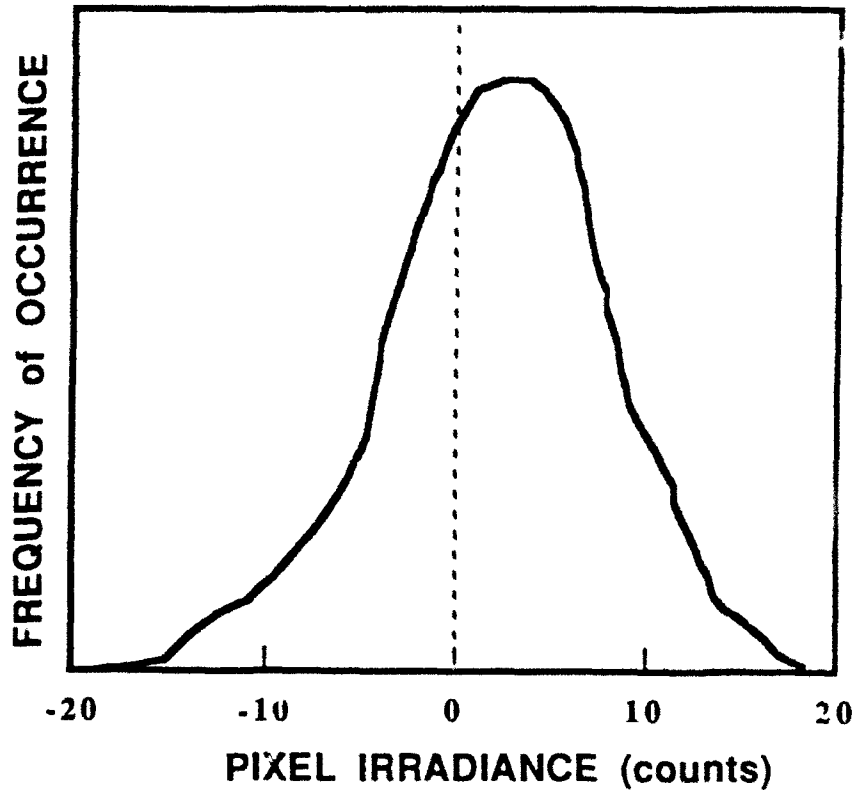


*Figure A.1 Typical histogram plot of uncorrected irradiance at null.*

## A.2 PEAK IRRADIANCE ESTIMATION

For a uniformly illuminated circular aperture, the diffraction-limited beam profile is specified by the airy irradiance function

$$E_{Airy}(r) = Q\left(\frac{(kD/2f)^2}{4\pi}\right)\left[2\frac{J_1(kDr/2f)}{kDr/2f}\right]^2 \quad , \tag{A-3}$$

where D is the aperture diameter, f is the focal length of the telescope, and Q is the pulse energy. It will be convenient to approximate this function by the Gaussian

$$\begin{aligned} E_{Gauss}(r) &= Q\left(\frac{(kD/2f)^2}{4\pi}\right)\exp\left[-\frac{1}{2}\left(\frac{(kD/2f)^2}{2}\right)r^2\right] \\ &= \frac{Q}{2\pi\sigma_o^2}\exp\left[-\frac{1}{2}\left(\frac{r^2}{\sigma_o^2}\right)\right] \quad , \end{aligned} \tag{A-4}$$

where $\sigma_o^2 = 2\left(\frac{2f}{kD}\right)^2$ defines the Gaussian beam width.

The beam profile of an aberrated beam might be modeled in the following way

$$E(r) = \frac{QS}{2\pi\sigma_o^2}\exp\left[-\frac{1}{2}\left(\frac{r^2}{\sigma^2}\right)\right] \quad , \tag{A-5}$$

where S is the peak irradiance (the usual definition of Strehl) and $\sigma$ is the beam diameter (which will usually be larger than $\sigma_o$). The irradiance can be treated as a probability density from which a distribution function can be formed

$$F(r) = 2\pi\int_0^r E(r)\,r\,dr \approx QS\left(\frac{\sigma^2}{\sigma_o^2}\right)\left\{1 - \exp\left[-\frac{1}{2}\left(\frac{r^2}{\sigma^2}\right)\right]\right\} \tag{A-6}$$

and

$$F(E) \approx QS\left(\frac{\sigma^2}{\sigma_o^2}\right) - 2\pi\sigma^2 E \quad . \tag{A-7}$$

The function F(E) represents the total focal plane energy attributed to those pixels exceeding the

irradiance threshold E. F(E) is seen to be a linear function of the irradiance, with a slope that is proportional to the beam radius $\sigma$. The x–axis intercept $E_p \equiv QS/2\pi\sigma_o^2$ provides a means to measure of the peak irradiance, while the y–axis intercept gives the total energy included in the Gaussian core. Therefore, a linear fit to the upper portion of the irradiance distribution function will generate estimates of both the Strehl and the effective beam diameter. The general appearance of the F(E) curves for diffraction limited and aberrated beams are illustrated in Figure A-2. The knee of the curve will generally occur well below the $E_p/2$ point, so it is usually safe to include all data points above this value in the linear regression operation.

The preceding derivation provides a working definition of the Strehl ratio that includes the following analysis steps:

1. the formation of the corrected camera-data histogram h(I),
2. the creation of the camera distribution function $F(I) = \sum_{i \geq I} i\, h(i)$,
3. the development of a linear fit to the upper half of the F(I) curve to obtain F'(I), and
4. the determination of the x-axis intercept Ip for which F'(Ip) = 0.

The Strehl ratio is now defined to be

$$S = \frac{2\pi\, \sigma_o^2\, I_p}{\sum_x \sum_y I(x,y)} \quad . \tag{A-8}$$

As usual, the determination of Strehl requires an accurate measurement of the total pulse energy and knowledge of the camera's magnification. Observe that

$$2\pi\, \sigma_o^2 = \frac{4}{\pi}\left(\frac{\lambda f}{Dd}\right)^2 = \frac{4}{\pi}\left(\frac{\Delta}{n}\right)^2 \quad , \tag{A-9}$$

where d is the pixel dimension, n is the number of phase sensor subapertures, and $\Delta$ is a magnification factor given in units of beam motion (pixels) per wave of tilt per subaperture. Since the Strehl is proportional to $\Delta^2$, it is important that this magnification factor is remeasured following each change to the optical arrangement.

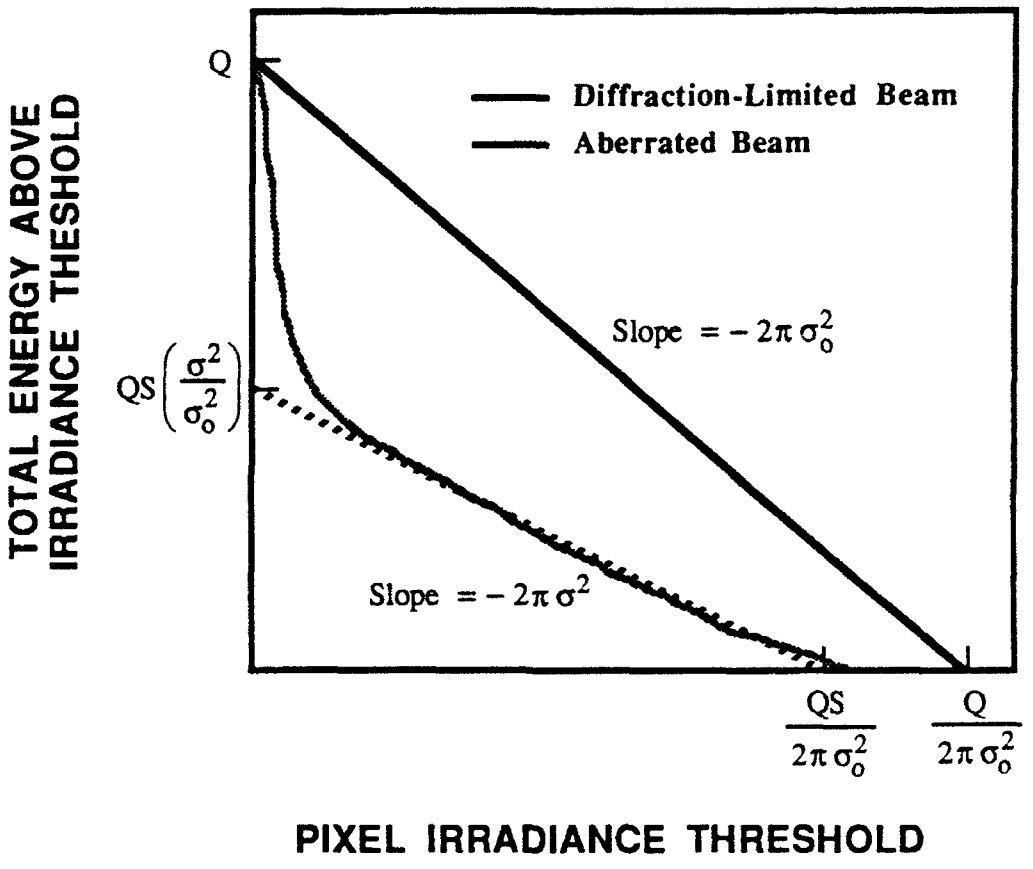


*Figure A.2 Energy distribution functions for diffraction-limited and aberrated beams.*

# REPORT DOCUMENTATION PAGE

*Form Approved*
*OMB No. 0704-0188*



| 1. AGENCY USE ONLY (*Leave blank*) | 2. REPORT DATE | 3. REPORT TYPE AND DATES COVERED |
|---|---|---|
| | 10 March 1993 | Project Report |

**4. TITLE AND SUBTITLE**

SWAT Laboratory Test Results

**5. FUNDING NUMBERS**

C — F19628-90-C-0002
PE — 63217C, 63221C
PR — 33

**6. AUTHOR(S)**

Ronald R. Parenti and Daniel V. Murphy

**7. PERFORMING ORGANIZATION NAME(S) AND ADDRESS(ES)**

Lincoln Laboratory, MIT
P.O. Box 73
Lexington, MA 02173-9108

**8. PERFORMING ORGANIZATION REPORT NUMBER**

PR-SWP-6, Revision 1

**9. SPONSORING/MONITORING AGENCY NAME(S) AND ADDRESS(ES)**

AF Phillips Laboratory
Kirtland Air Force Base
Albuquerque, NM 87177-6008

**10. SPONSORING/MONITORING AGENCY REPORT NUMBER**

ESC-TR-92-143

**11. SUPPLEMENTARY NOTES**

None

**12a. DISTRIBUTION/AVAILABILITY STATEMENT**

Approved for public release; distribution is unlimited.

**12b. DISTRIBUTION CODE**

**13. ABSTRACT** (*Maximum 200 words*)

The non-cooperative-target beam-control problem has been the subject of intense investigation since the synthetic-beacon concept was first introduced to the high-energy-laser community in 1982. While numerous analytical studies and computer simulations have been performed to evaluate the practical utility of this phase-measurement technique, prior to Lincoln Laboratory's SWAT (Short-Wavelength Adaptive Techniques) program, no experimental verification had been obtained. In the first phase of the SWAT investigation, completed in 1985, a high degree of correlation between differential-phase measurements from natural and artificial sources was demonstrated.

The next phase of the SWAT program will be performed at the AMOS (Air Force Maui Optical Station) facility in Maui, where a 241-actuator adaptive-optics system and an array of six dye lasers will be integrated with the site's 60-cm beam director. Prior to shipment, the adaptive-optics subsystem was subjected to a thorough laboratory evaluation, which culminated in a series of compensation tests involving simulated beacon sources. The results of these measurements are in good agreement with theoretical predictions and provide strong evidence of the efficacy of the synthetic-beacon approach.

| 14. SUBJECT TERMS | | 15. NUMBER OF PAGES |
|---|---|---|
| adaptive optics | phase conjugation | 56 |
| atmospheric turbulence | synthetic beacon | 16. PRICE CODE |
| laser guide star | | |

| 17. SECURITY CLASSIFICATION OF REPORT | 18. SECURITY CLASSIFICATION OF THIS PAGE | 19. SECURITY CLASSIFICATION OF ABSTRACT | 20. LIMITATION OF ABSTRACT |
|---|---|---|---|
| Unclassified | Unclassified | Unclassified | Same As Report |